

# RSC Advances



This is an *Accepted Manuscript*, which has been through the Royal Society of Chemistry peer review process and has been accepted for publication.

*Accepted Manuscripts* are published online shortly after acceptance, before technical editing, formatting and proof reading. Using this free service, authors can make their results available to the community, in citable form, before we publish the edited article. This *Accepted Manuscript* will be replaced by the edited, formatted and paginated article as soon as this is available.

You can find more information about *Accepted Manuscripts* in the [Information for Authors](#).

Please note that technical editing may introduce minor changes to the text and/or graphics, which may alter content. The journal's standard [Terms & Conditions](#) and the [Ethical guidelines](#) still apply. In no event shall the Royal Society of Chemistry be held responsible for any errors or omissions in this *Accepted Manuscript* or any consequences arising from the use of any information it contains.



## The promotional role of Ce in Cu/ZSM-5 and in situ surface reaction for selective catalytic reduction of NO<sub>x</sub> with NH<sub>3</sub>

Shuangshuang Lai, Wangcheng Zhan\*, Yun Guo, Yanglong Guo, Zhigang Zhang, Guanzhong Lu\*

Received 27th June 2015,  
Accepted 00th January 20xx

DOI: 10.1039/x0xx00000x

www.rsc.org/

Cu/ZSM-5 and Ce doped Cu/ZSM-5 catalysts were prepared by the incipient-wetness-impregnation method, and the effect of Ce doping on the structure and the catalytic performance of the Cu/ZSM-5 catalyst was investigated in detail for the selective catalytic reduction (SCR) of NO with NH<sub>3</sub>. The results showed that the addition of Ce can markedly broaden the operation temperature window of the Cu/ZSM-5 catalyst for NH<sub>3</sub>-SCR and enhance its H<sub>2</sub>O and SO<sub>2</sub> resistance. The presence of Ce promoted an enrichment of copper species (isolated Cu<sup>2+</sup> ions and CuO nanoparticles) on the catalyst surface and the increase in the Lewis acid sites on the surface of the Cu/ZSM-5 catalyst, and strengthened the redox property of the Cu/ZSM-5 catalyst. As a result, Ce-doped Cu/ZSM-5 catalyst possessed the high adsorption ability of NH<sub>3</sub> and nitrite/nitrate, which is propitious to the increase in the reactivity of the Ce-doped Cu/ZSM-5 catalyst. In situ DRIFTS results indicated that the NH<sub>3</sub>-SCR reaction on the Cu/ZSM-5 catalyst and Ce<sub>1</sub>-Cu<sub>4</sub>/ZSM-5 catalysts definitely followed Langmuir-Hinshelwood mechanisms, and bridged nitrates and bidentate nitrates were the active intermediate. However, Eley-Rideal mechanism can't be confirmed over the Cu/ZSM-5 and Ce<sub>1</sub>-Cu<sub>4</sub>/ZSM-5 catalysts.

### 1. Introduction

Nitrogen oxides (NO<sub>x</sub>) originated from various combustion processes are a kind of major air pollutants, which are very harmful to human health, due to the formation of photochemical smog, acid rain, ozone depletion and greenhouse effects. The selective catalytic reduction of NO<sub>x</sub> with ammonia (NH<sub>3</sub>-SCR) in the presence of excess oxygen has been considered as one of the best available approaches to control the emission of NO<sub>x</sub> produced from the stationary sources and the diesel vehicle. V<sub>2</sub>O<sub>5</sub>-WO<sub>3</sub>(MoO<sub>3</sub>)/TiO<sub>2</sub> behaves the high activity and selectivity of NH<sub>3</sub>-SCR and has been the most widely used in industry.<sup>1</sup> However, there are still some inevitable problems, such as the narrow working temperature window (300-400°C), the toxicity of vanadium species,<sup>2</sup> and the low N<sub>2</sub> selectivity at high temperatures.<sup>3</sup> Therefore, it is necessary to develop vanadium-free catalysts with high SCR activity.

In recent years, the zeolite-based catalysts are considered to be a practical solution for reducing the exhaust pollutants from diesel engines, and exhibit the high activities and good stability at high temperatures,<sup>4,5</sup> especially the Cu/ZSM-5 catalyst due to its superior SCR activity and N<sub>2</sub> selectivity in a wide temperature range.<sup>6</sup> However, previous researches indicated that the Cu/ZSM-5 catalyst did not possess a high SCR activity

at high temperature.<sup>7</sup> With respect to monometallic copper loaded catalysts, it is difficult to enhance its SCR activity simply by increasing the copper content in the Cu/ZSM-5 catalyst. This is because a high content of copper inevitably leads to agglomeration of the copper species and formation of large copper oxide particles,<sup>8</sup> which would enhance the oxidation of NH<sub>3</sub> and narrow the temperature window. It has been determined that the optimal content of copper in the Cu/ZSM-5 catalyst is within 3-4 wt.%.<sup>9</sup>

Ceria has been studied extensively as an oxygen reservoir, which can store and release oxygen by the redox cycle between Ce<sup>3+</sup> and Ce<sup>4+</sup> under oxidizing and reducing conditions.<sup>10,11,12</sup> Many Ce doped catalysts were studied extensively and used in the various reactions, including CeO<sub>2</sub>-MnO<sub>x</sub>,<sup>10,13</sup> CeWO<sub>x</sub>,<sup>14</sup> Ce-Mn/ZSM-5,<sup>11</sup> and Ce-Cu/ZSM-5.<sup>15,16</sup> Recently, it was reported that Ce-Cu/ZSM-5 catalyst was used for NH<sub>3</sub>-SCR reaction. Pang et al.<sup>17</sup> reported that adding Ce into Cu/ZSM-5 monolithic catalyst could obviously improve its activity and hydrothermal stability by stabilizing the dispersion of CuO and suppressing the formation of bulk-type CuO crystallites during hydrothermal treatment. Dou et al.<sup>18</sup> also confirmed that Ce doping improved the redox properties of the Cu-Ce/ZSM-5 catalyst, due to the higher valence of copper and mobility of lattice oxygen than those of Cu/ZSM-5 catalyst. But little attention has been paid to the effect of Ce doping on

Key Laboratories for Advanced Materials, Research Institute of Industrial Catalysis, East China University of Science and Technology, 130 Meilong Road, Shanghai 200237, China. E-mail: gzhl@ecust.edu.cn, zhanwc@ecust.edu.cn; Fax: +86-21-64252923

the acid sites, surface species and adsorption property of Ce-Cu/ZSM-5 catalysts. And the surface reaction mechanism over the Ce-Cu/ZSM-5 catalyst for the NH<sub>3</sub>-SCR reaction and the role of Ce on the catalytic cycle has not been investigated.

Herein, we try to solve two problems for Ce doped Cu/ZSM-5 catalysts, the promotional role of Ce and the surface reaction mechanism over the Ce-Cu/ZSM-5 catalyst for the NH<sub>3</sub>-SCR reaction, including the effect of Ce doping on the SO<sub>2</sub> resistance and water resistance. These research results will certainly be useful for the further development of the zeolite catalysts for the NH<sub>3</sub>-SCR reaction.

## 2. Experimental

### 2.1 Preparation of catalysts

A series of Ce<sub>x</sub>-Cu<sub>4</sub>/ZSM-5 catalysts with copper content of 4wt% and variable content of cerium were prepared by an improved incipient-wetness-impregnation method. H-ZSM-5 with Si/Al atomic ratio of 18 was supplied by Nankai University, Tianjin, China. In a typical process, the required amount of an aqueous solution of Cu(NO<sub>3</sub>)<sub>2</sub>·3H<sub>2</sub>O and Ce(NO<sub>3</sub>)<sub>3</sub>·6H<sub>2</sub>O was slowly dropped into the support under vigorous stirring at room temperature, and then ultrasonically treated for 1 h. The content of copper in the catalysts was maintained at 4wt%, and the content of cerium was varied. The solid was dried at 120 °C for 12 h and calcined in air at 550 °C for 4 h. The final catalysts were labeled as Ce<sub>x</sub>-Cu<sub>4</sub>/ZSM-5 (x denotes the weight ratio of Ce/H-ZSM-5, x = 0.5, 1, 2wt.%).

The Cu<sub>4</sub>/ZSM-5 catalyst was also prepared with the same procedure as Ce<sub>x</sub>-Cu<sub>4</sub>/ZSM-5, but no Ce(NO<sub>3</sub>)<sub>3</sub>·6H<sub>2</sub>O was added in the synthesis solution.

### 2.2 Catalyst characterization

The XRD patterns were recorded on a Brook/D8 diffractometer with CuKα Radiation (λ=0.154056 nm) in the 2θ range of 5–60°. The morphologies of the catalysts were investigated by field emission scanning electron microscopy (FE-SEM) on a Hitachi S-4800 instrument operated at the beam energy of 15 kV. The N<sub>2</sub> adsorption-desorption isotherms were measured on a Quantachrome NOVA1200 surface area at -196 °C. Prior to the measurements, all samples were degassed at 180 °C until a stable vacuum of ca. 5 mTorr was reached. The surface areas of the samples were calculated by Brunauer-Emmett-Teller (BET) method. The pore size distribution were calculated from the desorption branch using the Barrett-Joyner-Halenda (BJH) method. The XPS spectra were recorded on a Thermo ESCALAB 250 spectrometer with a monochromatized AlKα X-ray source (1486.6 eV) and a passing energy of 25 eV. C1s (binding energy 284.6 eV) of adventitious carbon was used as the reference.

Py-IR spectra of samples were analyzed by a Nicolet 5700 FT-IR spectrometer. The samples (13 mg) was heated at 400 °C under vacuum for 2h, and cooled to 200 °C when pyridine was chemisorbed for 10 min. After this step, the sample was evacuated and analyzed by FTIR.

Temperature-programmed desorption of NH<sub>3</sub> (NH<sub>3</sub>-TPD) was carried out on a PX200 apparatus (Tianjin Pengxiang Technology Ltd. China) with a thermal conductivity detector

(TCD). 50 mg of the sample was filled into the quartz reactor and pretreated at 500 °C in a flow of N<sub>2</sub> (50 mL/min) for 1 h. After being cooled down to room temperature, the sample was exposed to a flow of 10% NH<sub>3</sub>/N<sub>2</sub> (50 mL/min) for 0.5 h. Then the sample was flushed by N<sub>2</sub> (50 mL/min) for 1 h and NH<sub>3</sub>-TPD was carried out by heating the sample in N<sub>2</sub> (50 mL/min) from room temperature to 800 °C at 10 °C/min.

NO-TPD was carried out on the custom-made equipment with a NO<sub>x</sub> analyzer (Thermo Fisher Model 42i-HL NO-NO<sub>x</sub>-chemiluminescence analyzer) as detector. The sample was pretreated in Ar (450 ml/min) at 450 °C for 1 h and cooled down to room temperature. Then the sample was exposed to a flow of 500 ppm NO/Ar (300 mL/min) for 1 h to reach saturated adsorption of NO on the sample, followed by Ar (300 mL/min) purging for 1 h. Finally, NO-TPD was carried out by heating the sample in Ar (300 mL/min) from room temperature to 450 °C at 10 °C/min.

Temperature-programmed reduction with H<sub>2</sub> (H<sub>2</sub>-TPR) was performed in a conventional flow apparatus. 100 mg of the sample was used. A flow of 5% H<sub>2</sub>/N<sub>2</sub> (40 mL/min) was passed through the catalyst bed at 10 °C/min from 30 to 600 °C. The consumption of hydrogen was monitored by a thermal conductivity detector (TCD).

The in situ DRIFT measurements were performed on a Nicolet 6700 FT-IR spectrometer with a MCT detector. The sample was pretreated at 500 °C in Ar for 1 h, and then cooled to 150 °C in Ar. The background spectra were recorded at the different temperatures during the cooling, and background was subtracted from sample spectra accordingly.

### 2.3 Catalytic activity testing

The catalytic activities of the Ce<sub>x</sub>-Cu<sub>4</sub>/ZSM-5 catalysts for NH<sub>3</sub>-SCR in excess oxygen were investigated in a fixed-bed quartz reactor (Φ 6 mm × 300 mm). 200 mg of the catalyst (20-40 mesh) was used. The reactant gas was composed of 500 ppm NO, 500 ppm NH<sub>3</sub>, 5 vol% O<sub>2</sub>, 2 vol% H<sub>2</sub>O (when used), 50 ppm SO<sub>2</sub> (when used) and balanced Ar. The gas hourly space velocity (GHSV) was 55000 h<sup>-1</sup>. The concentrations of NO and NO<sub>x</sub> remained in the product were analysed by a Thermo Fisher NO-NO<sub>x</sub>-chemiluminescence analyzer. To avoid modest errors caused by the oxidation of ammonia in the converter of NO/NO<sub>x</sub> analyzer, an ammonia trap containing phosphoric acid solution was installed prior to the chemiluminescence detector. NO<sub>x</sub> conversion X(NO<sub>x</sub>) was calculated as follows:

$$X(\text{NO}_x) = \frac{[\text{NO}_x]_{in} - [\text{NO}_x]_{out}}{[\text{NO}_x]_{in}} \times 100\%$$

## 3. Results and discussion

### 3.1 Catalytic performance for NH<sub>3</sub>-SCR activity

The catalytic activities of the Cu<sub>4</sub>/ZSM-5 and Ce<sub>x</sub>-Cu<sub>4</sub>/ZSM-5 catalysts for the NH<sub>3</sub>-SCR reaction are shown in Fig.1. The H-ZSM-5 catalyst exhibited a very low activity, over which the maximum NO<sub>x</sub> conversion is only 80% at 425 °C. The Cu<sub>4</sub>/ZSM-5 catalyst has a high catalytic activity, and the NO<sub>x</sub> conversion of above 90% was obtained at 195 ~ 435 °C.

When cerium was added to  $\text{Cu}_4/\text{ZSM-5}$ , the catalytic activity of  $\text{Cu}_4/\text{ZSM-5}$  toward  $\text{NH}_3\text{-SCR}$  reaction was significantly improved, especially at the high temperature. For example, when the  $\text{Ce}_1\text{-Cu}_4/\text{ZSM-5}$  catalyst was used, the temperature window of more than 90%  $\text{NO}_x$  conversion was 185–470 °C; while for the  $\text{Ce}_2\text{-Cu}_4/\text{ZSM-5}$  and  $\text{Ce}_{0.5}\text{-Cu}_4/\text{ZSM-5}$  catalysts, their window were 180–460 °C and 175–450 °C, respectively. The results clearly demonstrate that comparing with the operation window of  $\text{Cu}_4/\text{ZSM-5}$  catalyst, adding an appropriate amount of Ce in this catalyst can broaden the operation window about 45 °C. Furthermore, the amount of Ce obviously affects the  $\text{NH}_3\text{-SCR}$  activity of the  $\text{Ce}_x\text{-Cu}_4/\text{ZSM-5}$  catalyst at the high temperature, while this influence is faint at the low temperature.

On the other hand, both the  $\text{Cu}_4/\text{ZSM-5}$  and  $\text{Ce}_1\text{-Cu}_4/\text{ZSM-5}$  catalysts behaved the high stability after the  $\text{NH}_3\text{-SCR}$  reaction. As shown in Fig. S1, the  $\text{NH}_3\text{-SCR}$  activities of the  $\text{Cu}_4/\text{ZSM-5}$  and  $\text{Ce}_1\text{-Cu}_4/\text{ZSM-5}$  catalysts on the second run are almost the same as those on the first run.

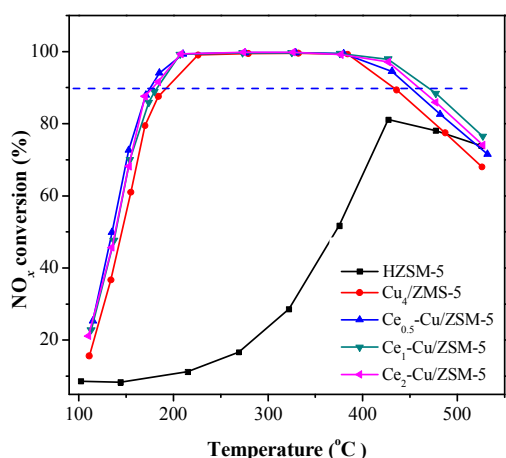


Fig. 1.  $\text{NO}_x$  conversion as a function of the reaction temperature over  $\text{Cu}_4/\text{ZSM-5}$  and  $\text{Ce}_x\text{-Cu}_4/\text{ZSM-5}$  catalysts for the  $\text{NH}_3\text{-SCR}$  reaction. (Reaction conditions: 0.2g catalyst, the reactant gas of 500 ppm  $\text{NO}/500$  ppm  $\text{NH}_3/5\%\text{O}_2/\text{Ar}$  balanced, GHSV = 55000  $\text{h}^{-1}$ ).

### 3.2 Physicochemical properties of catalysts

Fig. 2 shows the XRD patterns of H-ZSM-5,  $\text{Cu}_4/\text{ZSM-5}$  and  $\text{Ce}_x\text{-Cu}_4/\text{ZSM-5}$  catalysts. All the samples exhibit the typical diffraction peaks of ZSM-5 zeolite at  $2\theta = 7.9^\circ$ ,  $8.8^\circ$ ,  $23.1^\circ$  and  $23.8^\circ$ , which represent the (011), (020), (051) and (033) planes, respectively.<sup>19</sup> Comparing with the XRD spectrum of H-ZSM-5, the XRD spectra of  $\text{Cu}_4/\text{ZSM-5}$  and  $\text{Ce}_x\text{-Cu}_4/\text{ZSM-5}$  catalysts were changed inconspicuously, which indicates that the structure of zeolite support remains intact after adding Cu and Ce. On the other hand, the diffraction peaks of CuO are not detected for all catalysts, showing that the copper species are well dispersed on the surface of the ZSM-5 support, or aggregated crystallites are too small to be detected by XRD. Similarly, the diffraction peaks of  $\text{CeO}_2$  are not also detected for the  $\text{Ce}_x\text{-Cu}_4/\text{ZSM-5}$  catalysts with low Ce content. However, with increasing the Ce content to 2.0 wt.%, the very weak diffraction peak of  $\text{CeO}_2$  can be observed ( $2\theta = 28.2^\circ$ ) for the

$\text{Ce}_2\text{-Cu}_4/\text{ZSM-5}$  catalyst, indicating the formation of  $\text{CeO}_2$  crystallites on the surface of the  $\text{Ce}_2\text{-Cu}_4/\text{ZSM-5}$  catalyst.

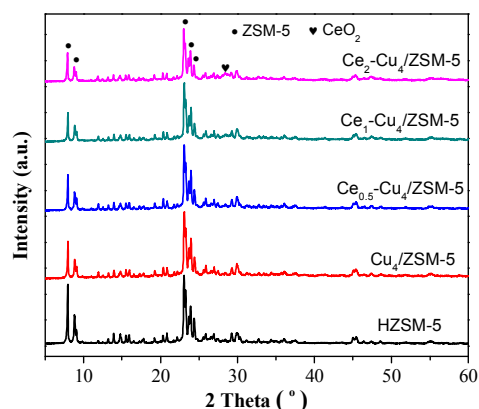


Fig. 2. Wide-angle XRD patterns of pure H-ZSM-5,  $\text{Cu}_4/\text{ZSM-5}$  and  $\text{Ce}_x\text{-Cu}_4/\text{ZSM-5}$  catalysts.

Fig. 3 shows the SEM images of H-ZSM-5,  $\text{Cu}_4/\text{ZSM-5}$  and  $\text{Ce}_1\text{-Cu}_4/\text{ZSM-5}$  catalysts. The results show that, H-ZSM-5 exhibits the schistose and irregular morphology, and after the addition of Cu and Ce, the morphologies of  $\text{Cu}_4/\text{ZSM-5}$  and  $\text{Ce}_x\text{-Cu}_4/\text{ZSM-5}$  catalysts are virtually unchanged. The BET surface area, average pore diameter and micro-pore volume are listed in Table 1. It can be seen that adding Cu leads to the decrease in BET surface area, average pore diameter and micro-pore volume, which can be attributed to the fact that copper species cover the external surface of H-ZSM-5, blocking many zeolite channels. After the addition of Ce into the  $\text{Cu}_4/\text{ZSM-5}$  catalyst, BET surface area was decreased slightly, while average pore diameter and micro-pore volume remained unchanged.

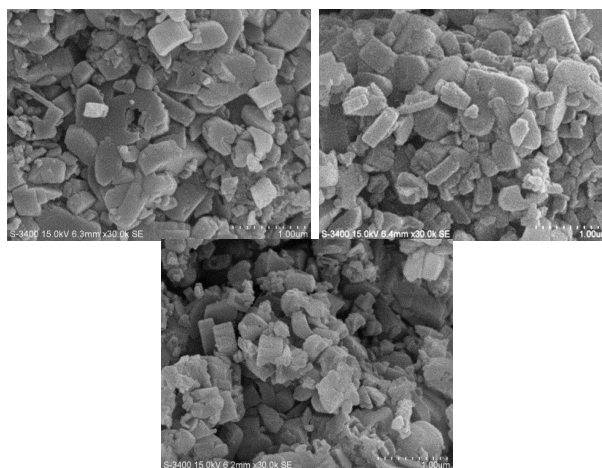


Fig. 3. SEM images of pure H-ZSM-5 (top left),  $\text{Cu}_4/\text{ZSM-5}$  (top right) and  $\text{Ce}_1\text{-Cu}_4/\text{ZSM-5}$  (bottom).

Fig. 4 shows XPS  $\text{Cu}2p$  spectra of  $\text{Cu}_4/\text{ZSM-5}$  and  $\text{Ce}_1\text{-Cu}_4/\text{ZSM-5}$  catalysts. The  $\text{Cu}_4/\text{ZSM-5}$  catalyst has two main peaks at BE = 933.6 eV and 953.0 eV in its XPS  $\text{Cu}2p$  spectra, which are attributed to  $\text{Cu}2p_{3/2}$  and  $\text{Cu}2p_{1/2}$ , respectively. The  $\text{Cu}2p_{3/2}$  peaks can be deconvoluted to two peaks, and the peaks at 933.4 eV represent the agglomerated CuO nanoparticles on

## ARTICLE

## RSC Advances

the surface of catalysts, and the one at BE = 935.2 eV is attributed to isolated  $\text{Cu}^{2+}$  ion coordinated to superficial oxygen atoms of zeolite.<sup>18,20</sup> Since the diffraction peaks of CuO species could not be observed in the XRD spectra, these CuO crystallites' size should be lower than 3 nm.

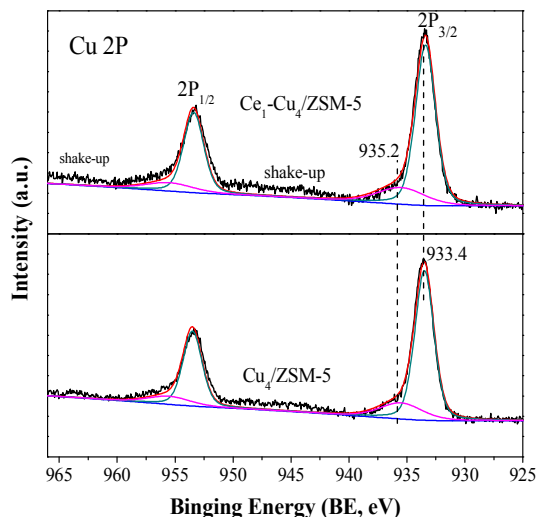


Fig. 4. XPS Cu2p spectra of  $\text{Cu}_4/\text{ZSM-5}$  and  $\text{Ce}_1\text{-Cu}_4/\text{ZSM-5}$  catalysts.

Table 1 shows the surface atom concentrations of  $\text{Cu}_4/\text{ZSM-5}$  and  $\text{Ce}_1\text{-Cu}_4/\text{ZSM-5}$  catalysts. It can be seen that surface Cu amount increases with the addition of Ce in the  $\text{Cu}_4/\text{ZSM-5}$  catalyst, indicating that the presence of Ce can help to the enrichment of Cu on the  $\text{Cu}_4/\text{ZSM-5}$  surface. According to the peak area ratio of (isolated  $\text{Cu}^{2+}$  ions)/(CuO crystallites) in XPS spectra, the amounts of isolated  $\text{Cu}^{2+}$  ions and CuO crystallites on the surface of  $\text{Cu}_4/\text{ZSM-5}$  and  $\text{Ce}_1\text{-Cu}_4/\text{ZSM-5}$  catalysts were calculated (Table 1). The results show that CuO crystallites are predominant on the surface of both  $\text{Cu}_4/\text{ZSM-5}$  and  $\text{Ce}_1\text{-Cu}_4/\text{ZSM-5}$  catalysts with a high Cu content, which is consistent with the reported results.<sup>20</sup> Furthermore, the surface concentrations of isolated  $\text{Cu}^{2+}$  ions and CuO crystallites over the  $\text{Ce}_1\text{-Cu}_4/\text{ZSM-5}$  catalyst are higher than that over the  $\text{Cu}_4/\text{ZSM-5}$  catalyst, because of the increase of the surface Cu atoms after Ce addition in the  $\text{Cu}_4/\text{ZSM-5}$  catalyst.

Table 1. BET surface area ( $S_{\text{BET}}$ ) and surface atom concentrations of the  $\text{Cu}_4/\text{ZSM-5}$  and  $\text{Ce}_1\text{-Cu}_4/\text{ZSM-5}$  catalysts derived from XPS data

Sample	$S_{\text{BET}}$ ( $\text{m}^2/\text{g}$ )	Average pore diameter (nm)	Micro-pore volume ( $\text{cm}^3/\text{g}$ )	isolated $\text{Cu}^{2+}/\text{CuO}^a$	Surface composition (At.%)		
					Cu (isolated $\text{Cu}^{2+}/\text{CuO}$ ) <sup>b</sup>	Ce	O
H-ZSM-5	333	2.1	0.14	-	-	-	-
$\text{Cu}_4/\text{ZSM-5}$	280	1.6	0.12	0.239	1.59 (0.31/1.28)	/	63.2
$\text{Ce}_1\text{-Cu}_4/\text{ZSM-5}$	268	1.6	0.12	0.247	1.97 (0.39/1.58)	0.25	62.8

<sup>a</sup> The peak area ratio (m) of M(isolated  $\text{Cu}^{2+}$  ions)/M(CuO crystallites) in XPS spectrum; <sup>b</sup> "isolated  $\text{Cu}^{2+}$ " was calculated by  $\text{Cu}(\text{at.}\%)\times(m/(1+m))$  and "CuO" was calculated by  $\text{Cu}(\text{at.}\%)/(1+m)$ .

Wang et al.<sup>21</sup> thought both CuO nanoparticles and isolated  $\text{Cu}^{2+}$  ion in  $\text{Cu}/\text{SAPO-34}$  were active sites for the  $\text{NH}_3\text{-SCR}$  reaction. Furthermore, it is revealed that the CuO nanoparticles catalyzes the oxidation of NO to  $\text{NO}_2$ , and this favors the reduction of NO at lower temperature due to the facilitation of the "fast SCR" process, while isolated  $\text{Cu}^{2+}$  ions help to the high NO conversion at high temperature. Therefore, when adding Ce in the  $\text{Cu}_4/\text{ZSM-5}$  catalyst, the increase in the surface concentrations of both isolated  $\text{Cu}^{2+}$  ions and CuO nanoparticles can improve the activity of the  $\text{Cu}_4/\text{ZSM-5}$  catalyst.

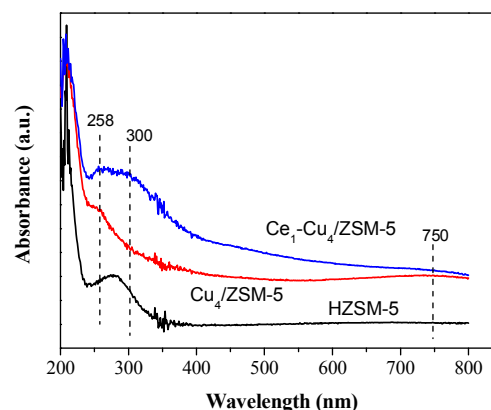


Fig. 5. UV-Vis spectra of HZSM-5,  $\text{Cu}_4/\text{ZSM-5}$  and  $\text{Ce}_1\text{-Cu}_4/\text{ZSM-5}$  catalysts.

Fig. 5 shows the UV-Vis absorption spectra of HZSM-5,  $\text{Cu}_4/\text{ZSM-5}$  and  $\text{Ce}_1\text{-Cu}_4/\text{ZSM-5}$  catalysts. HZSM-5 exhibits the adsorption bands at about 210 and 280 nm. For  $\text{Cu}_4/\text{ZSM-5}$ , a band at 258 nm and a broad band centered at 750 nm between 550 and 800 nm appeared. The former can be assigned to  $\text{O}\rightarrow\text{Cu}$  transitions of isolated  $\text{Cu}^{2+}$  ions in coordination with lattice oxygen, and the latter can be assigned to d-d transitions of  $\text{Cu}^{2+}$  ions in an octahedrally coordinated environment due to dispersed CuO crystallites on

the catalyst surface.<sup>22-24</sup> When cerium was added to Cu<sub>4</sub>/ZSM-5, a broad band centered at 300 nm appeared, which can be attributed to well-dispersed Ce species on the surface of catalyst (presumably in a tetra-coordinated environment), which is confirmed by the XRD results.<sup>25</sup> Meanwhile, the intensity of 258 nm band was increased compared with that in UV-Vis spectra of Cu<sub>4</sub>/ZSM-5 catalyst, indicating the increase in the amount of isolated Cu<sup>2+</sup> ions, which is consistent with the XPS results. On the contrary, it is difficult to quantify CuO crystallites on the catalyst surface because two bands centered at 300 and 750 nm overlap complexity.

### 3.3 Temperature-programmed desorption

Fig.6 shows NH<sub>3</sub>-TPD profiles of the H-ZSM-5, Cu<sub>4</sub>/ZSM-5 and Ce<sub>1</sub>-Cu<sub>4</sub>/ZSM-5 catalysts in the temperature range of 100~500 °C. Two desorption peaks at 200 and 410 °C can be observed for the H-ZSM-5 catalyst. The desorption peak at 200 °C is assigned to physisorbed NH<sub>3</sub> or ammonium species, and the desorption peak at 410 °C is assigned to NH<sub>3</sub> adsorbed at the strong acid sites.<sup>26</sup>

After adding copper and cerium, the NH<sub>3</sub>-TPD profiles have been obviously changed. The desorption peak at 410 °C radically decreased for the Cu<sub>4</sub>/ZSM-5 and Ce<sub>1</sub>-Cu<sub>4</sub>/ZSM-5 catalysts. On the contrary, a shoulder peak at 306 °C presented for the Cu<sub>4</sub>/ZSM-5 and Ce<sub>1</sub>-Cu<sub>4</sub>/ZSM-5 catalysts. The reasons for this phenomena were because part of Brønsted acid protons were substituted by metal ion and strong Lewis acid sites were produced originating from metal oxide nanoparticles when adding Cu and/or Ce into the H-ZSM-5 catalyst.<sup>27,28</sup> Compared with the Cu<sub>4</sub>/ZSM-5 catalyst, the peak area at 306 °C is slightly larger for the Ce<sub>1</sub>-Cu<sub>4</sub>/ZSM-5 catalyst, even if the specific surface area was considered, because the BET surface area (268 m<sup>2</sup>/g) of the former is less than that (280 m<sup>2</sup>/g) of the latter, indicating that the Ce<sub>1</sub>-Cu<sub>4</sub>/ZSM-5 catalyst possessed the more strong acid sites than that on the Cu<sub>4</sub>/ZSM-5 catalyst.

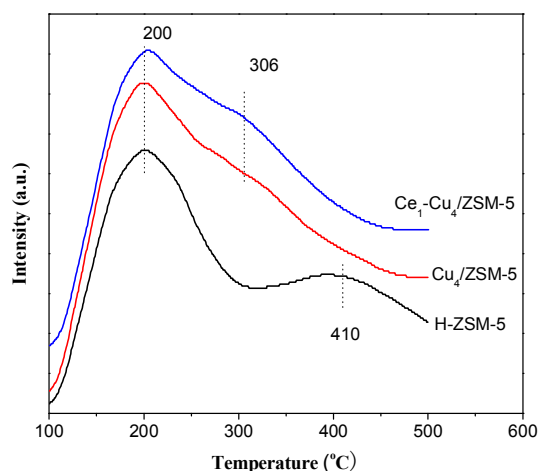


Fig. 6. NH<sub>3</sub>-TPD profiles of H-ZSM-5, Cu<sub>4</sub>/ZSM-5 and Ce<sub>1</sub>-Cu<sub>4</sub>/ZSM-5 catalysts.

Fig.7 shows IR spectra of adsorbed pyridine on H-ZSM-5, Cu<sub>4</sub>/ZSM-5 and Ce<sub>1</sub>-Cu<sub>4</sub>/ZSM-5 catalysts. The absorption bands

at 1450 cm<sup>-1</sup> and 1545 cm<sup>-1</sup> are assigned to Lewis acid sites and Brønsted acid sites respectively, while the absorption band at 1490 cm<sup>-1</sup> is assigned to both them. The concentration of the Lewis acid sites (LA) and Brønsted acid sites (BA) were calculated from the intensity of the absorption bands at 1450 cm<sup>-1</sup> and 1545 cm<sup>-1</sup>, and the results are shown in Table 2. It can be seen that the H-ZSM-5 catalyst mainly exhibited Brønsted acid sites. After adding copper, the amount of Brønsted acid sites markedly decreased due to the ion exchange during the preparation step. On the contrary, the amount of Lewis acid sites increased largely because of the presence of Cu<sup>2+</sup> ions on the surface. Furthermore, compared with the H-ZSM-5 catalyst, the Cu<sub>4</sub>/ZSM-5 catalyst possessed the higher amount of total acid sites. When adding cerium into the Cu<sub>4</sub>/ZSM-5 catalyst, the amounts of both the Lewis acid sites and Brønsted acid sites were increased, leading to the higher amount of total acid sites, which is in accordance with the NH<sub>3</sub>-TPD results. It has been proved that Brønsted acid sites may not be required for activating ammonia, while Lewis acid sites plays an important role on the NH<sub>3</sub>-SCR process catalyzed by the zeolite catalyst.<sup>29</sup> Therefore, the more Lewis acid sites over the Ce<sub>1</sub>-Cu<sub>4</sub>/ZSM-5 catalyst might make the higher NH<sub>3</sub>-SCR activity of Ce<sub>1</sub>-Cu<sub>4</sub>/ZSM-5 than the Cu<sub>4</sub>/ZSM-5 catalyst.

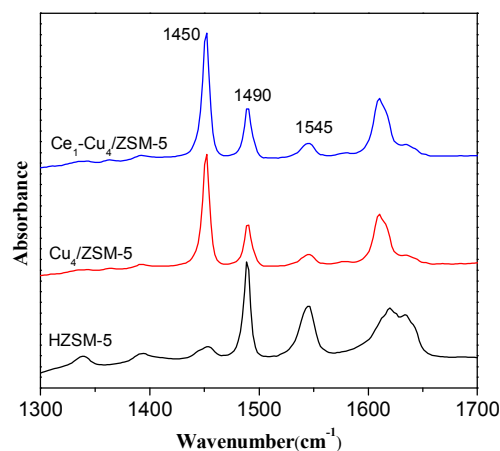


Fig. 7. IR spectra of adsorbed pyridine on H-ZSM-5, Cu<sub>4</sub>/ZSM-5 and Ce<sub>1</sub>-Cu<sub>4</sub>/ZSM-5 catalysts.

Table 2. Acidity of the H-ZSM-5, Cu<sub>4</sub>/ZSM-5 and Ce<sub>1</sub>-Cu<sub>4</sub>/ZSM-5 catalysts derived from IR spectra of adsorbed pyridine

Sample	LA <sup>a</sup> (μmol/mg)	BA <sup>b</sup> (μmol/mg)	Total of acid sites (μmol/mg)
H-ZSM-5	0.41	2.10	2.52
Cu <sub>4</sub> /ZSM-5	2.75	0.42	3.17
Ce <sub>1</sub> -Cu <sub>4</sub> /ZSM-5	3.08	0.54	3.62

<sup>a</sup> The Lewis acid sites; <sup>b</sup> The Brønsted acid sites.

The NO-TPD profiles of the catalysts are also shown in Fig. 8. Two obvious desorption peaks centered at 120 and 400 °C presented in the NO-TPD profile of the Cu<sub>4</sub>/ZSM-5 catalyst. The

## ARTICLE

## RSC Advances

desorption peak at 120 °C can be attributed to physisorbed  $\text{NO}_x$ , and the desorption peak at 400 °C is due to the decomposition of nitrite and nitrate species with higher thermal stability.<sup>30</sup> After adding Ce in the  $\text{Cu}_4/\text{ZSM-5}$  catalyst, the desorption peak area at 400 °C increased remarkably, indicating that the addition of Ce can enhance the adsorption of nitrite and nitrate species on the surface of the  $\text{Cu}_4/\text{ZSM-5}$  catalyst. In addition, the presence of Ce in this catalyst also improves the adsorption capacity and ability for NO at low temperature. As a result, more nitrite and nitrate species on the  $\text{Ce}_1\text{-Cu}_4/\text{ZSM-5}$  catalyst surface can participate the SCR reaction than that on the surface of the  $\text{Cu}_4/\text{ZSM-5}$  catalyst, and the Ce doped catalyst can adsorb NO at lower temperature, resulting in the enhancement of the catalytic activity and the extension of the operation temperature window of the  $\text{Ce}_1\text{-Cu}_4/\text{ZSM-5}$  catalyst.

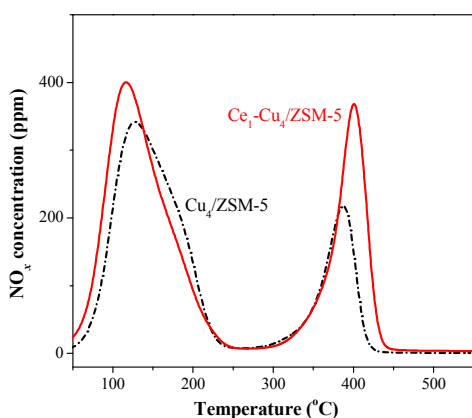


Fig. 8. NO-TPD profiles of the  $\text{Cu}_4/\text{ZSM-5}$  and  $\text{Ce}_1\text{-Cu}_4/\text{ZSM-5}$  catalysts

### 3.4 $\text{H}_2$ -TPR

Fig. 9 shows  $\text{H}_2$ -TPR profiles of H-ZSM-5,  $\text{Cu}_4/\text{ZSM-5}$  and  $\text{Ce}_1\text{-Cu}_4/\text{ZSM-5}$  catalysts. The H-ZSM-5 catalyst does not exhibit any reduction peaks. There are three reduction peaks at 213, 245 and 330 °C in the TPR profile of the  $\text{Cu}_4/\text{ZSM-5}$  catalyst. The reduction peak at 213 °C is attributed to the reduction of CuO nanoparticles dispersed on the ZSM-5 surface to  $\text{Cu}^0$ , and the reduction peaks at 245 and 330 °C are assigned to the reduction of isolated  $\text{Cu}^{2+}$  to  $\text{Cu}^0$  through two steps.<sup>31</sup> The reduction  $\text{Cu}^{2+} \rightarrow \text{Cu}^+$  can occur at lower temperature, and the reduction  $\text{Cu}^+ \rightarrow \text{Cu}^0$  only can carry out at higher temperature. For the  $\text{Ce}_1\text{-Cu}_4/\text{ZSM-5}$  catalyst, there are also three reduction peaks, the peak at 330 °C shifted to a higher temperature of 350 °C, and the reduction peak area at 213 °C was markedly increased comparing with the  $\text{Cu}_4/\text{ZSM-5}$  catalyst, due to the high surface concentrations of CuO nanoparticles (Table 1). The results above show that adding Ce in the  $\text{Cu}_4/\text{ZSM-5}$  catalyst can enhance its reducibility.

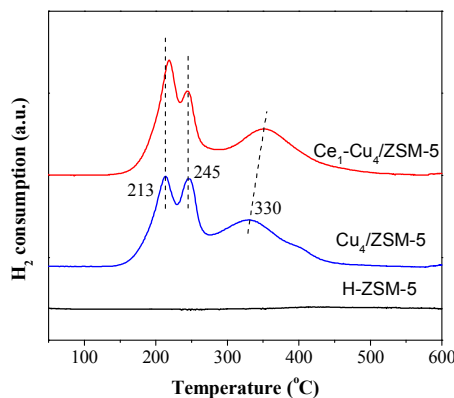


Fig. 9.  $\text{H}_2$ -TPR profiles of H-ZSM-5,  $\text{Cu}_4/\text{ZSM-5}$  and  $\text{Ce}_1\text{-Cu}_4/\text{ZSM-5}$  catalysts.

### 3.5 NO oxidation

It is well known that the improvement of NO oxidation to  $\text{NO}_2$  over SCR catalysts can significantly promote its low temperature activity, due to the occurrence of the “fast SCR”,  $\text{NO} + \text{NO}_2 + 2\text{NH}_3 \rightarrow 2\text{N}_2 + 3\text{H}_2\text{O}$ .<sup>32</sup> Therefore, the effect of adding Ce on the catalytic activity of the  $\text{Cu}_4/\text{ZSM-5}$  catalyst for NO oxidation has been investigated. As shown in Fig. 10, for the NO oxidation at < 400 °C, the activity of the  $\text{Ce}_1\text{-Cu}_4/\text{ZSM-5}$  catalyst is slightly higher than that of the  $\text{Cu}_4/\text{ZSM-5}$  catalyst, due to the higher reducibility of the  $\text{Ce}_1\text{-Cu}_4/\text{ZSM-5}$  catalyst. At the high temperature, there is no difference of the catalytic activity of both catalysts for NO oxidation because of the equilibrium conversion.

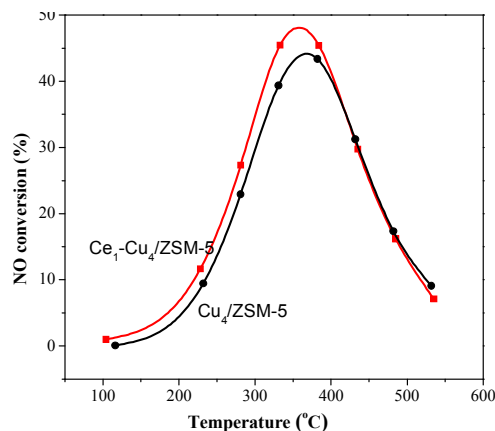


Fig. 10. NO conversion in separate NO oxidation reaction over the  $\text{Cu}_4/\text{ZSM-5}$  and  $\text{Ce}_1\text{-Cu}_4/\text{ZSM-5}$  catalysts. (Reaction conditions: 500 ppm NO + 5 vol.%  $\text{O}_2/\text{Ar}$  balanced, total flow rate 300 mL/min).

### 3.6 In situ DRIFT spectroscopy

#### 3.6.1 Adsorption of $\text{NH}_3$ followed by introduction of $\text{NO} + \text{O}_2$

Prior to  $\text{NH}_3$  adsorption, the catalyst was pretreated at 500 °C in the Ar flow of 50 mL/min for 1 h and cooled to 150 °C, and then the catalyst was exposed to the gas of 500 ppm  $\text{NH}_3/\text{Ar}$  (50 mL/min) at 150 °C, while in situ DRIFT spectra of the  $\text{Cu}_4/\text{ZSM-5}$  (or  $\text{Ce-Cu}_4/\text{ZSM-5}$ ) catalyst were taken for different times, and the DRIFT spectra of  $\text{NH}_3$  adsorbed on catalysts are presented in Fig. 11.

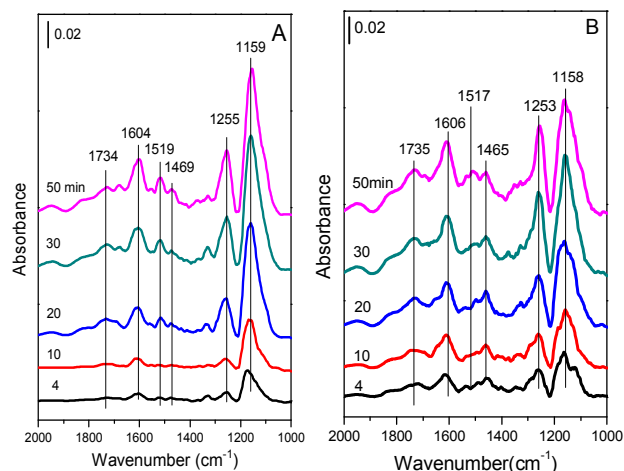


Fig. 11. In situ DRIFT spectra of (A)  $\text{Cu}_4/\text{ZSM-5}$  and (B)  $\text{Ce}_1\text{-Cu}_4/\text{ZSM-5}$  catalysts exposed to a flow of 500 ppm  $\text{NH}_3/\text{Ar}$  (50 mL/min) at 150 °C for different times.

The bands at 1159 and 1255, 1604  $\text{cm}^{-1}$  are assigned to coordinated  $\text{NH}_3$  adsorbed on Lewis acid sites, the bands at 1469 and 1734  $\text{cm}^{-1}$  are assigned to  $\text{NH}_4^+$  ions located on Brønsted acid sites.<sup>19,33-36</sup> And the band at 1519  $\text{cm}^{-1}$  might be attributed to amide ( $-\text{NH}_2$ ) species.<sup>19,37</sup> With an increase in the exposure time, the intensities of all bands are obviously increased, indicating the increase in the amount of adsorbed  $\text{NH}_3$  species. After adding Ce in the  $\text{Cu}_4/\text{ZSM-5}$  catalyst, its in situ DRIFT spectra are similar to that of the  $\text{Cu}_4/\text{ZSM-5}$  catalyst. The coordinated  $\text{NH}_3$  adsorbed on Lewis acid sites (bands at 1158, 1253 and 1606  $\text{cm}^{-1}$ ), and  $\text{NH}_4^+$  ions located on Brønsted acid sites (bands at 1469 and 1734  $\text{cm}^{-1}$ ) are also presented, and their intensities are increased obviously with the increase in the exposure time of  $\text{NH}_3$ . As shown in Fig.11, Lewis acid sites on the two catalysts are dominant to adsorb or activate  $\text{NH}_3$  compared with Brønsted acid sites, because most of Brønsted acid sites have been substituted by Ce or Cu ions.<sup>38</sup>

After the experiments of Fig. 11 were finished, the catalyst was purged with Ar (50 mL/min) for 1h, and then was exposed to 500 ppm  $\text{NO} + 5 \text{ vol.}\% \text{O}_2/\text{Ar}$  (50 mL/min). In situ DRIFT spectra of the catalyst were taken for different times and are presented in Fig. 12.

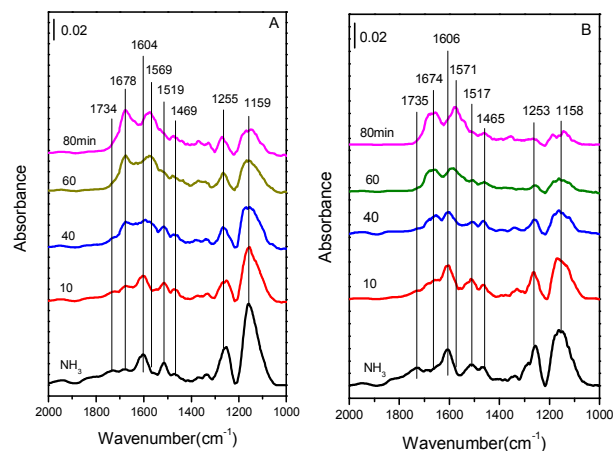


Fig. 12. In situ DRIFT spectra of (A)  $\text{Cu}_4/\text{ZSM-5}$  and (B)  $\text{Ce}_1\text{-Cu}_4/\text{ZSM-5}$  catalysts in the mixed gas of 500 ppm  $\text{NO} + 5 \text{ vol.}\% \text{O}_2/\text{Ar}$  at different times, after adsorption of 500 ppm  $\text{NH}_3/\text{Ar}$  at 150 °C and blowing by Ar for 1 h.

As shown in Fig. 12A, when  $\text{NO} + \text{O}_2$  is exposed to  $\text{NH}_3$ -pretreated  $\text{Cu}_4/\text{ZSM-5}$  catalyst, the intensities of the bands at 1159, 1255, 1604, 1519 and 1734  $\text{cm}^{-1}$  decreased gradually with the increase in the exposure time of  $\text{NO} + \text{O}_2$ , which indicates that both  $\text{NH}_3$  species adsorbed on Lewis acid sites and  $\text{NH}_4^+$  ions located on Brønsted acid sites are involved in the  $\text{NH}_3\text{-SCR}$  reaction. At the same time, many new bands at 1678 and 1569  $\text{cm}^{-1}$  ascribed to nitrates species appeared and increased with the increase of the exposure time in  $\text{NO} + \text{O}_2$ . After adding Ce, the bands assigned to adsorbed  $\text{NH}_3$  species decreased more quickly on the  $\text{Ce}_1\text{-Cu}_4/\text{ZSM-5}$  catalyst with the increase in the exposure time of  $\text{NO} + \text{O}_2$  (Fig. 12B), indicating the higher SCR activity compared with the  $\text{Cu}_4/\text{ZSM-5}$  catalyst.

### 3.6.2 Adsorption of $\text{NO} + \text{O}_2$ followed by introduction of $\text{NH}_3$

Prior to the adsorption of  $\text{NO} + \text{O}_2$ , the catalyst was pretreated at 500 °C in Ar (50 ml/min) for 1 h. After the catalyst was cooled down to 150 °C, Ar gas was replaced by the mixed gas of 500 ppm  $\text{NO} + 5 \text{ vol.}\% \text{O}_2/\text{Ar}$  (50 ml/min), and in situ DRIFT spectra of the  $\text{Cu}_4/\text{ZSM-5}$  and  $\text{Ce}_1\text{-Cu}_4/\text{ZSM-5}$  catalysts were taken for different times, and their results are shown in Fig. 13. As shown in Fig. 13A, there are three strong bands at 1679, 1628 and 1568  $\text{cm}^{-1}$  in the DRIFT spectra of the  $\text{Cu}_4/\text{ZSM-5}$  catalyst. The bands at 1628 and 1568  $\text{cm}^{-1}$  are assigned to bridged and bidentate nitrates respectively,<sup>39-42</sup> and the band at 1679  $\text{cm}^{-1}$  is attributed to ionic nitrite species.<sup>43,44</sup> These bands were increased with the exposure time. Besides, there are still three bands with low intensity at 1438, 1303 and 1200  $\text{cm}^{-1}$  in the DRIFT spectra of the  $\text{Cu}_4/\text{ZSM-5}$  catalyst. These bands are assigned to nitrite species.<sup>42,44,45</sup>

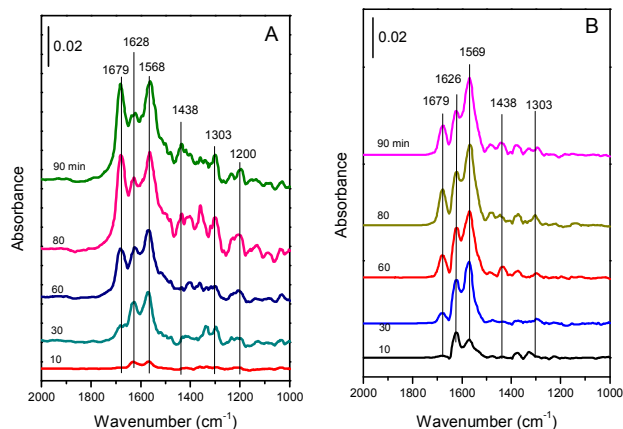


Fig. 13. In situ DRIFT spectra of the (A)  $\text{Cu}_4/\text{ZSM-5}$  and (B)  $\text{Ce}_1\text{-Cu}_4/\text{ZSM-5}$  catalysts exposed to a flow of 500 ppm  $\text{NO} + 5 \text{ vol.}\% \text{O}_2/\text{Ar}$  (50 mL/min) at 150 °C for different times.

Compared with the in situ DRIFT spectra of the  $\text{Cu}_4/\text{ZSM-5}$  catalyst, the strong absorption bands at 1679, 1626 and 1569  $\text{cm}^{-1}$  are also shown in the in situ DRIFT spectra of the  $\text{Ce}_1\text{-Cu}_4/\text{ZSM-5}$  catalyst (Fig. 13B), but the intensity of the absorption band at 1679  $\text{cm}^{-1}$  corresponding to ionic nitrite species is much lower than those at 1626 and 1569  $\text{cm}^{-1}$ . This



is because that the higher oxidation of the  $Ce_1-Cu_4/ZSM-5$  catalyst (as shown in  $H_2$ -TPR results) can easily oxidize ionic nitrite species to nitrates, resulting in the reduction in the ionic nitrite species on the  $Ce_1-Cu_4/ZSM-5$  catalyst surface. At the same time, the intensities of the bands at 1438 and  $1303\text{ cm}^{-1}$  are much low, and the band at  $1200\text{ cm}^{-1}$  assigned to bridged nitrite has even disappeared. Since nitrates are the active species for the SCR reaction, the highly catalytic activity of the  $Ce_1-Cu_4/ZSM-5$  catalyst for the oxidation of nitrite to nitrate is favorable for the better SCR activity.

To study the reaction between  $NH_3$  and adsorbed  $NO_x$  species, after the experiments of Fig. 13 were finished, the catalyst was purged with Ar (50 mL/min) for 1h, and then was exposed to 500 ppm  $NH_3/Ar$  (50 mL/min). In situ DRIFT spectra of the catalyst were taken for different times and their results are presented in Fig. 14.

As shown in Fig.14A, the intensities of the bands at  $1568\text{ cm}^{-1}$  (assigned to bidentate nitrate) and  $1628\text{ cm}^{-1}$  (assigned to bridged nitrate) decreased quickly with the increase of the exposure time in 500 ppm  $NH_3$ , indicating that bidentate and bridged nitrates are the reactive species with a high activity for the SCR reaction. On the contrast, the intensity of band at  $1679\text{ cm}^{-1}$  (assigned to ionic nitrite species) was hardly changed even after  $NH_3$  was passed over the catalyst for 80 min, showing that this species is inactive in SCR process. Simultaneously, the bands at 1159, 1255 and  $1606\text{ cm}^{-1}$  originating from  $NH_3$  adsorption species appear, and their intensities increase with the increase of the exposure time in  $NH_3$ .

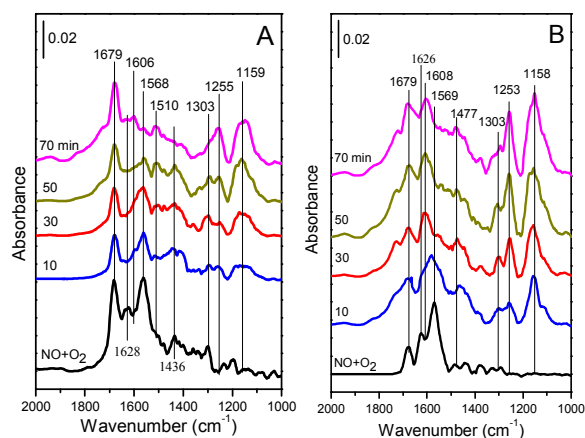


Fig. 14. In situ DRIFT spectra over (A)  $Cu_4/ZSM-5$  and (B)  $Ce_1-Cu_4/ZSM-5$  catalysts in 500 ppm  $NH_3/Ar$  for different times after adsorption of 500 ppm  $NO + 5\text{ vol.}\% O_2/Ar$  at  $150^\circ C$  and blowing by Ar for 1 h.

Like the DRIFT results of the  $Cu_4/ZSM-5$  catalyst, the intensities of the bands at  $1569\text{ cm}^{-1}$  and  $1626\text{ cm}^{-1}$  over the  $Ce_1-Cu_4/ZSM-5$  catalyst decreased with the increase in the exposure time of  $NH_3$ , and these two bands disappeared after 30 min, which is less than that for the disappearance of these two bands over the  $Cu_4/ZSM-5$  catalyst (60 min), indicating a high SCR activity of the  $Ce_1-Cu_4/ZSM-5$  catalyst. On the contrary, the variation of the band at  $1679\text{ cm}^{-1}$  was unobvious with the time. At the same time, the bands at 1158, 1253, 1477 and  $1608\text{ cm}^{-1}$  originating from  $NH_3$  adsorption

species appeared, and their intensities increased with the increase of the exposure time in  $NH_3$ . Compared with the DRIFT results of the  $Cu_4/ZSM-5$  catalyst, the intensities of the bands assigned to  $NH_3$  adsorption species over the  $Ce_1-Cu_4/ZSM-5$  catalyst are higher.

### 3.6.3 Proposed reaction pathway

As shown in Fig. 11,  $NH_3$  mainly adsorbed on Lewis acid sites, as well as a little on Brønsted acid sites, and both  $NH_3$  species adsorbed on Lewis acid sites and Brønsted acid sites are involved in the  $NH_3$ -SCR reaction. As a result, the bands corresponding to  $NH_3$  adsorption in in situ DRIFT spectra (Fig. 12) decreased gradually when the catalysts pretreated with  $NH_3$  are exposed to the mixed gas of  $NO$  and  $O_2$ .

For the  $Ce_1-Cu_4/ZSM-5$  catalyst, the bands assigned to adsorbed  $NH_3$  species on the  $Ce_1-Cu_4/ZSM-5$  catalyst was decreased more quickly with the increase in the exposure time of  $NO + O_2$  (Fig. 12B), indicating its higher SCR activity than the  $Cu_4/ZSM-5$  catalyst. As shown in Fig. 13, the  $NO$  species can adsorb on the surface of the  $Cu_4/ZSM-5$  and  $Ce_1-Cu_4/ZSM-5$  catalysts in the forms of bridged and bidentate nitrates, ionic nitrite and nitrate, and bridged nitrite. The nitrite species tend to be oxidized to nitrate species over the  $Ce_1-Cu_4/ZSM-5$  catalyst, because of its high catalytic activity for the oxidation reaction. When the catalysts pretreated with the mixed gas of  $NO$  and  $O_2$  were exposed to  $NH_3$ , bidentate nitrate and bridged nitrate were consumed very quickly, while ionic nitrite species was hardly changed. These results indicate that bidentate nitrate and bridged nitrate over the  $Cu_4/ZSM-5$  and  $Ce_1-Cu_4/ZSM-5$  catalysts are the reactive species with a high SCR reactivity, and the SCR reaction is followed Langmuir-Hinshelwood mechanism over the  $Cu_4/ZSM-5$  and  $Ce_1-Cu_4/ZSM-5$  catalysts.

As above mentioned, when the catalysts pretreated with the mixed gas of  $NO$  and  $O_2$  were exposed to  $NH_3$ , bidentate nitrate and bridged nitrate consumed very quickly and disappeared after 30 or 60 min (Fig.14). However, when the catalysts pretreated with  $NH_3$  were exposed to the mixed gas of  $NO$  and  $O_2$ , the bands corresponding to  $NH_3$  adsorption in in situ DRIFT spectra (Fig. 12) decreased gradually, and a part of  $NH_3$  species adsorbed on the catalysts surface remained still after 80 min. Therefore, when the catalysts pretreated with  $NH_3$  were exposed to the mixed gas of  $NO$  and  $O_2$ ,  $NO$  maybe adsorbed on the surface of catalysts pretreated with  $NH_3$  firstly and then reacted with pre-adsorbed  $NH_3$ , resulting in the low reaction rate. Therefore, it can't be confirmed whether the SCR reaction over the  $Cu_4/ZSM-5$  and  $Ce_1-Cu_4/ZSM-5$  catalysts is followed Eley-Rideal mechanism.

### 3.7 Effect of $SO_2$ and $H_2O$ on the SCR reaction

Fig. 15 shows the effect of  $SO_2$  and  $H_2O$  on the catalytic activities of the  $Cu_4/ZSM-5$  and  $Ce_1-Cu_4/ZSM-5$  catalysts for the SCR reaction at  $200^\circ C$ . Before adding  $H_2O$  or  $SO_2$ ,  $NO_x$  conversion was 100% over the two catalysts and their activities was unchanged after 20 h of the reaction at  $200^\circ C$ . When 2%  $H_2O$  was introduced into the feed gas,  $NO_x$  conversion over the  $Cu_4/ZSM-5$  catalysts immediately decreased to 90.2% after 8 h of the reaction. After 2%  $H_2O$  in the feed gas was removed and

lasting for 2 h, the  $\text{NO}_x$  conversion was returned to  $\sim 100\%$ . After adding Ce in the  $\text{Cu}_4/\text{ZSM-5}$  catalyst, its performance for  $\text{H}_2\text{O}$  resistance was improved, for instance, the  $\text{NO}_x$  conversion could hold  $\sim 94\%$  in the presence of 2% water. And its  $\text{NO}_x$  conversion was returned to  $\sim 100\%$  after removing 2%  $\text{H}_2\text{O}$  in the feed gas and lasting for 1.5 h. A similar trend can also be observed at high reaction temperature ( $450^\circ\text{C}$ ) over the  $\text{Cu}_4/\text{ZSM-5}$  and  $\text{Ce}_1\text{-Cu}_4/\text{ZSM-5}$  catalysts (Fig S2).

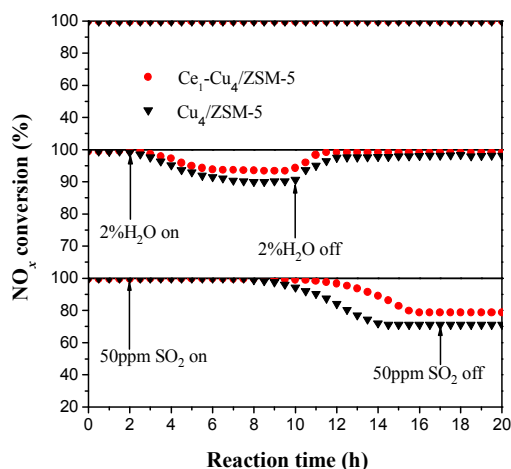


Fig.15. Effect of  $\text{SO}_2$  and  $\text{H}_2\text{O}$  on the catalytic activities of  $\text{Cu}_4/\text{ZSM-5}$  and  $\text{Ce}_1\text{-Cu}_4/\text{ZSM-5}$  catalysts for SCR reaction at  $200^\circ\text{C}$ . (Reaction conditions: 0.2 g catalyst, 500 ppm NO, 500 ppm  $\text{NH}_3$ , 5%  $\text{O}_2$ , Ar to balance, GHSV=5500h<sup>-1</sup>)

When 50 ppm  $\text{SO}_2$  was introduced into the feed gas, 100%  $\text{NO}_x$  conversion over the  $\text{Cu}_4/\text{ZSM-5}$  catalysts was kept for 8 h and then decreased to 70.4% after the reaction of 6 h, but the deactivation of catalyst poisoned by  $\text{SO}_2$  could not be recovered. However, it is obvious that the catalytic activity of the  $\text{Ce}_1\text{-Cu}_4/\text{ZSM-5}$  catalyst was less affected by  $\text{SO}_2$  than the  $\text{Cu}_4/\text{ZSM-5}$  catalyst, that is to say, the Ce doping can improve the  $\text{SO}_2$  resistance of the  $\text{Cu}_4/\text{ZSM-5}$  catalyst. A similar trend can also be observed at high reaction temperature over the  $\text{Cu}_4/\text{ZSM-5}$  and  $\text{Ce}_1\text{-Cu}_4/\text{ZSM-5}$  catalysts (Fig S2). It is well known that the ammonium sulfate and copper sulfate deposited on the catalyst surface can cover available active sites and block zeolite channels,<sup>46</sup> and they could not be decomposed and removed at  $200^\circ\text{C}$  on the catalyst surface,<sup>47</sup> resulting in a deactivation of catalyst. The presence of Ce in the  $\text{Cu}_4/\text{ZSM-5}$  catalyst can make  $\text{SO}_2$  firstly deposit on the Ce site to form a stable Ce sulfate, which can inhibit the formation of ammonium sulfate and copper sulfate on the catalyst surface in the SCR process, improving the excellent sulfur tolerance of the  $\text{Ce}_1\text{-Cu}_4/\text{ZSM-5}$  catalyst.

#### 4. Conclusions

In summary, the addition of Ce can markedly improve the catalytic activity of the  $\text{Cu}/\text{ZSM-5}$  catalyst for  $\text{NH}_3\text{-SCR}$  reaction and enhance its  $\text{SO}_2$  and water resistance. Adding Ce in the  $\text{Cu}_4/\text{ZSM-5}$  catalyst promoted the enrichment of copper species on the catalyst surface and increased the surface concentrations of both isolated  $\text{Cu}^{2+}$  ions and  $\text{CuO}$  crystallites,

resulting in the improvement of the redox properties and the  $\text{NO}$  adsorption ability of the  $\text{Cu}_4/\text{ZSM-5}$  catalyst. The Ce amount would affect the catalytic performance of  $\text{Ce}_x\text{-Cu}/\text{ZSM-5}$ , especially the  $\text{NH}_3\text{-SCR}$  activity at high temperature. When the  $\text{Ce}_1\text{-Cu}_4/\text{ZSM-5}$  catalyst ( $\text{Ce}/\text{Cu} = 1/4$ , wt.) was used, the temperature window for more than 90%  $\text{NO}_x$  conversion was extended to  $185\sim 470^\circ\text{C}$ , which broadened the operation window about  $45^\circ\text{C}$ , because more nitrite and nitrate species on the  $\text{Ce}_1\text{-Cu}_4/\text{ZSM-5}$  catalyst surface can participate the SCR reaction than that on the surface of the  $\text{Cu}_4/\text{ZSM-5}$  catalyst, and the Ce-doping sample can adsorb  $\text{NO}$  at lower temperature. In situ DRIFTS results indicated that the Langmuir-Hinshelwood mechanism for the  $\text{NH}_3\text{-SCR}$  reaction over the  $\text{Cu}_4/\text{ZSM-5}$  and  $\text{Ce}_1\text{-Cu}_4/\text{ZSM-5}$  catalysts was confirmed, but Eley-Rideal mechanism can't be sure yet.

#### Acknowledgements

This work was supported financially by the National Natural Science Foundation of China (21577034, 21333003), the Commission of Science and Technology of Shanghai Municipality (15DZ1205305) and the Fundamental Research Funds for the Central Universities (WJ1514020).

#### Notes and references

1. A. Brückner, F. Hipler, G. Auer, E. Löffler, and W. Grünert, *J. Catal.*, 2012, 286, 237.
2. Z.M. Liu, J.H. Li, and S.I. Woo, *Energy Environ. Sci.*, 2012, 5, 8799.
3. W.P. Shan, F.D. Liu, H. He, X.Y. Shi, and C.B. Zhang, *Catal. Today*, 2012, 184, 160.
4. M.J. Li, Y. Yeom, E. Weitz, and W.M.H. Sachtler, *J. Catal.*, 2005, 235, 201.
5. X.F. Yang, Z.L. Wu, M. Moses-Debusk, D.R. Mullins, S.M. Mahurin, R.A. Geiger, M. Kidder, and C.K. Narula, *J. Phys. Chem. C.*, 2012, 116, 23322.
6. H. Sjövall, L. Olsson, E. Fridell, and R.J. Blint, *Appl. Catal. B*, 2006, 64, 180.
7. G. Carja, Y. Kameshima, K. Okada, and C.D. Madhusoodana, *Appl. Catal. B*, 2007, 73, 60.
8. J.L. De Lucas, F. Valverde, A. Dorado, and I. Romero, *J. Mol. Catal. A*, 2005, 225, 47.
9. J.H. Park, H.J. Park, J.H. Baik, I.S. Nam, C.H. Shin, J.H. Lee, B.K. Cho, and S.H. Oh, *J. Catal.*, 2006, 240, 47.
10. X.F. Tang, Y.G. Li, X.M. Huang, Y.D. Xu, H.Q. Zhu, J.G. Wang, and W.J. Shen, *Appl. Catal. B*, 2006, 62, 265.
11. G. Carja, Y. Kameshima, K. Okada, and C.D. Madhusoodana, *Appl. Catal. B*, 2007, 73, 60.
12. Z.B. Wu, R.B. Jin, Y. Liu, and H.Q. Wang, *Catal. Commun.*, 2008, 9, 2217.
13. S.M. Lee, K.H. Park, and S.C. Hong, *Chem. Eng. J.*, 2012, 195-196, 323.
14. K. Liu, F.D. Liu, L.J. Xie, W.P. Shan, H. He, *Catal. Sci. Technol.*, 2015, 5, 2290.

## ARTICLE

## RSC Advances

- 15 Y.P. Zhang, and M. Flytzani-Stephanopoulos, *J. Catal.*, 1996, 164, 131.
- 16 J.Y. Yan, W.M.H. Sachtler, and H.H. Kung, *Catal. Today*, 1997, 33, 279.
- 17 L. Pang, C. Fan, L.N. Shao, and K.P. Song, *Chem. Eng. J.*, 2014, 253, 394.
- 18 B.J. Dou, G. Lv, C. Wang, Q. Hao, K. Hui, *Chem. Eng. J.*, 2015, 270, 549.
- 19 F. Bin, *Appl. Catal. B*, 2014, 150-151, 532.
- 20 B. Pereda-Ayo, U.D.L. Torre, M.J. Illán-Gómez, A. Bueno-López, and J.R. González-Velasco, *Appl. Catal. B*, 2014, 147, 420.
- 21 L. Wang, J.R. Gaudet, W. Li, and D. Weng, *J. Catal.*, 2013, 306, 68.
- 22 M.H. Groothaet, J.A. van Bokhoven, A.A. Battiston, B.M. Weckhuysen, and R.A. Schoonheydt, *J. Am. Chem. Soc.*, 2003, 125, 7629
- 23 T. Zhang, J. Liu, D. Wang, Z. Zhao, Y. Wei, K. Cheng, G. Jiang, and A. Duan, *Appl. Catal. B*, 2014, 148-149, 520
- 24 S. Yashnik, and Z. Ismagilov, *Appl. Catal. B*, 2015, 170-171, 241.
- 25 Y. Fu, W. Zhan, Y. Guo, Y. Wang, X. Liu, Y. Guo, Y. Wang, and G. Lu, *Micropor. Mesopor. Mater.*, 2015, 214, 101
- 26 T. Zhang, J. Liu, D.X. Wang, Z. Zhao, Y.C. Wei, K. Cheng, G.Y. Jiang, and A.J. Duan, *Appl. Catal. B*, 2014, 148-149, 520.
- 27 G. H. Kuehl, H. and K. C. Timken, *Micropor Mesopor Mater.*, 2000, 35-36, 521.
- 28 L.J. Lobree, I.C. Hwang, J.A. Reimer, *J. Catal.* 186 (1999) 242-253
- 29 X. Liang, J. X. Li, Q. C. Lin, and K. Q. Sun, *Catal. Commun.*, 2007, 8, 1901.
- 30 X. D. Wu, F. Lin, H. and B. Xu, *Appl. Catal. B*, 2010, 96, 101.
- 31 A. De Lucas, J.L. Valverde, F. Dorado, A. Romero, and I. Asencio, *J Mol Catal A*, 2005, 225, 47.
- 32 J. Chen, M. Shen, X. Wang, G. Qi, J. Wang, and W. Li, *Appl. Catal B*, 2013, 251, 134.
- 33 *J Catal* 324 (j)98
- 34 *Topics in Catalysis* 56 (2013) 1441
- 35 *Catal. Today* 205 (2013) 16
- 36 *J Catal* 289 (2012) 21
- 37 W. S. Kijlstra, D. S. Brands, H. I. Smit, E. K Poels, and A. Bliet, *J. Catal.*, 1997, 171, 219.
- 38 S. Brandenberger, O. Kröcher, A. Wokaun, A. Tissler, and R. Althoff, *J. Catal.*, 2009, 268, 297.
- 39 W. Shan, F. Liu, H. He, X. Shi, and C. Zhang, *Appl. Catal. B*, 2012, 115-116, 100.
- 40 L. Shuang, W. Xiaodong, W. Duan and R. Rui, *Ind. Eng. Chem. Res.*, 2012, 51, 2271.
- 41 *ACB* 146(2014) 94
- 42 *PCCP* 15 (2013) 2368
- 43 K. Hadjiivanov, A. Penkova, M. Daturi, J. Saussey, and J. C. Lavalle, *Chem. Phys. Lett.*, 2003, 377, 642.
- 44 *Catal. Rev-Sci. Eng* 42 (2000) 71
- 45 I. Atribak, B. Azambre, A. Bueno López, and A. García-García, *Appl. Catal. B*, 2009, 92, 126.
- 46 Z.X. Ma, H.S. Yang, F. Liu, and X.B. Zhang, *Appl. Catal. A*, 2013, 467, 450.
- 47 J. Yu, F. Guo, Y.L. Wang, J.H. Zhu, Y.Y. Liu, and F.B. Su, *Appl Catal B*, 2010, 95, 160.